Study of $e^+e^- \to e^+e^-\eta'$ in the double-tag mode at BABAR

Evgeny Kozyrev

Novosibirsk State University

Budker INP SB RAS, Novosibirsk, Russia

on behalf of the BaBar collaboration

7th July 2018

Outline

- Introduction
  How the transition form factor (TFF) is defined?
  TFF at large momentum transfers
  TFF at small momentum transfers
  Existing experimental data
- Measurement of the TFF of η' meson with BaBar detector
- Comparison with theoretical predictions
- Summary

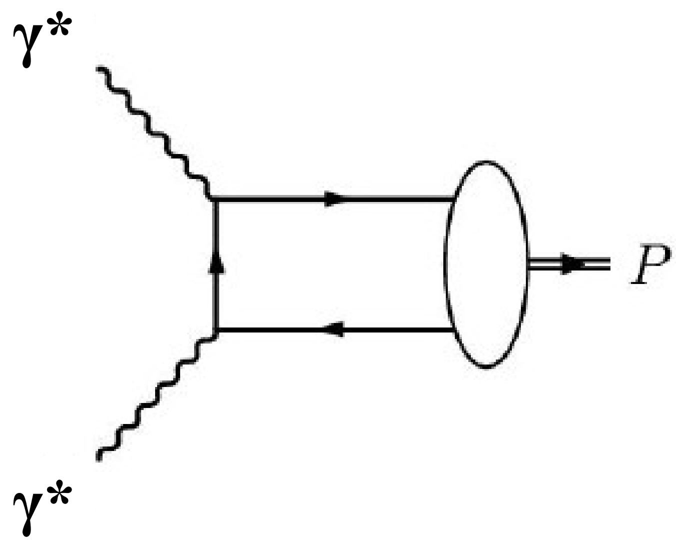

The amplitude of the $\gamma^*\gamma^*\to P$ transition

$$A = e^2 \varepsilon_{\mu\nu\alpha\beta} e_1^{\mu} e_2^{\nu} q_1^{\alpha} q_2^{\beta} F(q_1^2, q_2^2),$$

P — pseudoscalar meson
$e_{1,2}$ — photon polarization
$q_{1,2}$ — 4-momentum of photon

- there are a lot of experimental study of pseudoscalar meson production via the fusion of real (**on-shell**) and virtual (**off-shell**) photons
$\gamma^*\gamma \to$ **P**: π^0, η, η', η_c

- there are **no** measurements of the double **off-shell** transitions
$\gamma^*\gamma^* \to$ **P**

Introduction. $F(Q^2{}_1,Q^2{}_2)$ at large Q^2.

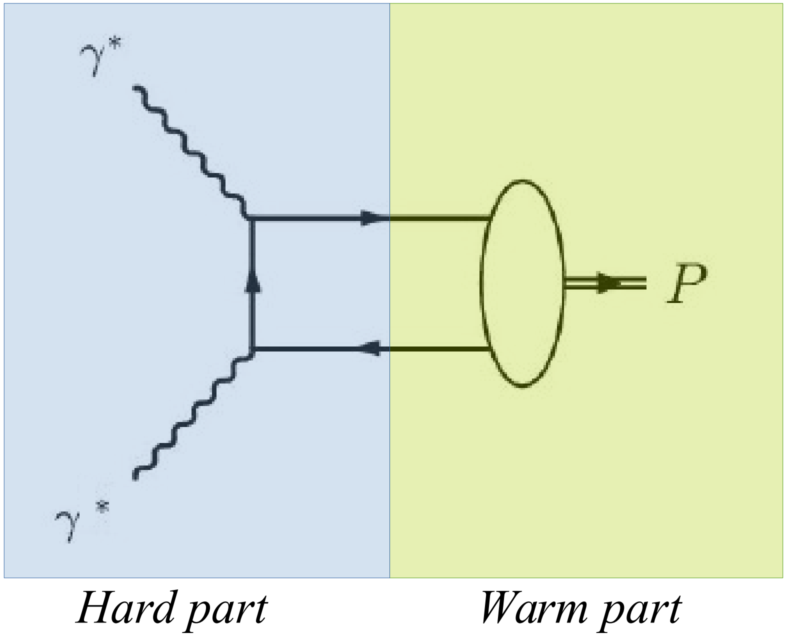

$$F(Q^2{}_1,Q^2{}_2) = \int T(x,Q^2{}_1,Q^2{}_2)\ \varphi(x,Q^2{}_1,Q^2{}_2)\ dx$$

x - is the fraction of the meson momentum carried by one of the quarks

$T(x,Q^2{}_1,Q^2{}_2)$ - hard scattering amplitude for $\gamma^*\gamma^*\rightarrow$qqbar transition which is calculable in pQCD

$\varphi(x,Q^2{}_1,Q^2{}_2)$ - nonperturbative meson distribution amplitude (DA) describing transition P → qqbar

$$T_H(x,Q_1^2,Q_2^2) = \frac{1}{2}\cdot\frac{1}{xQ_1^2+(1-x)Q_2^2}\cdot\left(1+C_F\frac{\alpha_S(Q^2)}{2\pi}\cdot t(x,Q_1^2,Q_2^2)\right)+(x\rightarrow 1-x)+O(\alpha_s^2)+O(\Lambda_{QCD}^4/Q^4)$$

NLO correction
[E. Braaten, Phys. Rev. D **28**, 3 (1983)]

- The meson DA **$\varphi(x,Q^2{}_1,Q^2{}_2)$** plays an important role in theoretical descriptions of many QCD processes. Its shape (x dependence) is unknown, but its evolution with **$\mu^2 = Q^2{}_1+Q^2{}_2$** is predicted by pQCD:

$$\mu^2\frac{d}{\mu^2}\phi(x,\mu) = \frac{\alpha_s(\mu)}{2\pi}\int_0^1 dyV(x,y)\phi(y,\mu)$$

At the limit **$\mu\rightarrow\infty$**

$$\phi_P(x,\mu) = A_P 6x(1-x)(1+O(\Lambda_{QCD}^2/\mu^2))$$

[S. J. Brodsky and G. P. Lepage, Phys. Rev. D 24, 7 (1981)]

- F(0,0) is related to axial anomaly:

$$\Gamma_{\eta'\to 2\gamma} = \frac{\pi\alpha^2 m^3_{\eta'}}{4}|F(0,0)|^2 = 4.30 \pm 0.16 \text{ keV} \quad \Rightarrow \quad F(0,0) = 0.342 \pm 0.006 \text{ GeV}^{-1}.$$

- The vector meson dominance model is commonly used to describe TFF at low Q^2:

$$F_{\eta'}(Q^2_1, Q^2_2) = \frac{F_{\eta'}(0,0)}{(1+Q^2_1/\Lambda^2_P)(1+Q^2_2/\Lambda^2_P)}$$

- In case of the TFF with one off-shell photon the pQCD and VMD models leads to the same asymptotic behaviour $F(Q^2) \propto 1/Q^2$ at $Q^2 \to \infty$.

-

	VMD	pQCD
$Q_1^2 \approx 0,\ Q_2^2 \to \infty$	$1/Q^2$	$1/Q^2$
$Q_1^2,\ Q_2^2 \to \infty$	$1/Q^4$	$1/Q^2$

A.V. Radyushkin, R. Ruskov, Nuclear Physics B 481 (1996) 625-680:

$$F^{LO}_{\gamma^*\gamma^*\pi^0}(q^2,Q^2) = \frac{4\pi}{3}\int_0^1 \frac{\varphi_\pi(x)}{xQ^2+\bar{x}q^2}\,dx, \tag{1.1}$$

where $\varphi_\pi(x)$ is the pion distribution amplitude and $x, \bar{x} \equiv 1-x$ are the fractions of the pion light-cone momentum carried by the quarks. In the region where both photon virtualities are large: $q^2 \sim Q^2 \gtrsim 1\ \mathrm{GeV}^2$, the pQCD predicts the overall $1/Q^2$ fall-off of the form factor, which differs from the naive vector meson dominance expectation $F_{\gamma^*\gamma^*\pi^0}(q^2,Q^2) \sim 1/q^2Q^2 \sim 1/Q^4$. Thus, establishing the $1/Q^2$ power law in this region is a crucial test of pQCD for this process. The study of $F_{\gamma^*\gamma^*\pi^0}(q^2,Q^2)$ over a wide range of the ratio q^2/Q^2 of two large photon virtualities can then provide non-trivial information about the shape of $\varphi_\pi(x)$.

Introduction. $F(Q^2_1,Q^2_2)$ at large Q^2.

$$F_{\eta'}(Q_1^2,Q_2^2) = \left(\frac{5\sqrt{2}}{9} f_n \sin\phi + \frac{2}{9} f_s \cos\phi\right)\int_0^1 dx\, \frac{1}{2}\frac{6x(1-x)}{xQ_1^2+(1-x)Q_2^2}\left(1 + C_F\frac{\alpha_s(\mu^2)}{2\pi}\cdot t(x,Q_1^2,Q_2^2)\right) + (x \to 1-x),$$

Master formula

The meson DA

NLO

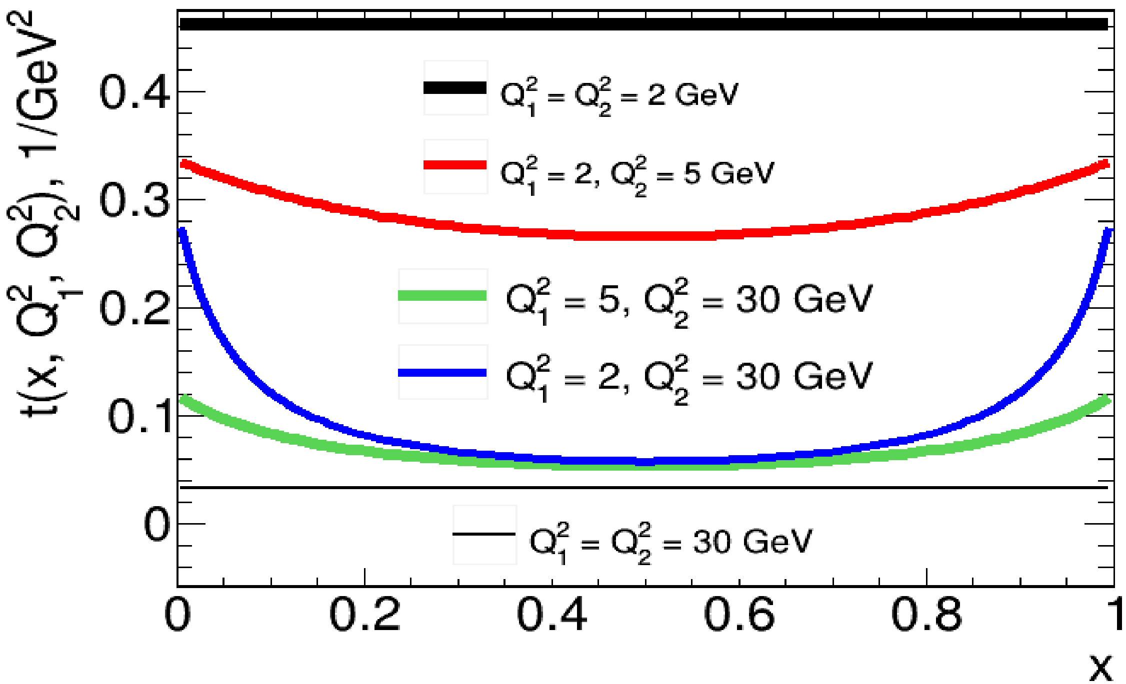

1. The double-virtual transition FF is less sensitive to NLO than the single-virtual one.

2. The form $1/[xQ_1^2+(1-x)Q_2^2]$ is not divergent, so double-virtual transition FF is less sensitive to a shape of the meson DA than the single-virtual FF.

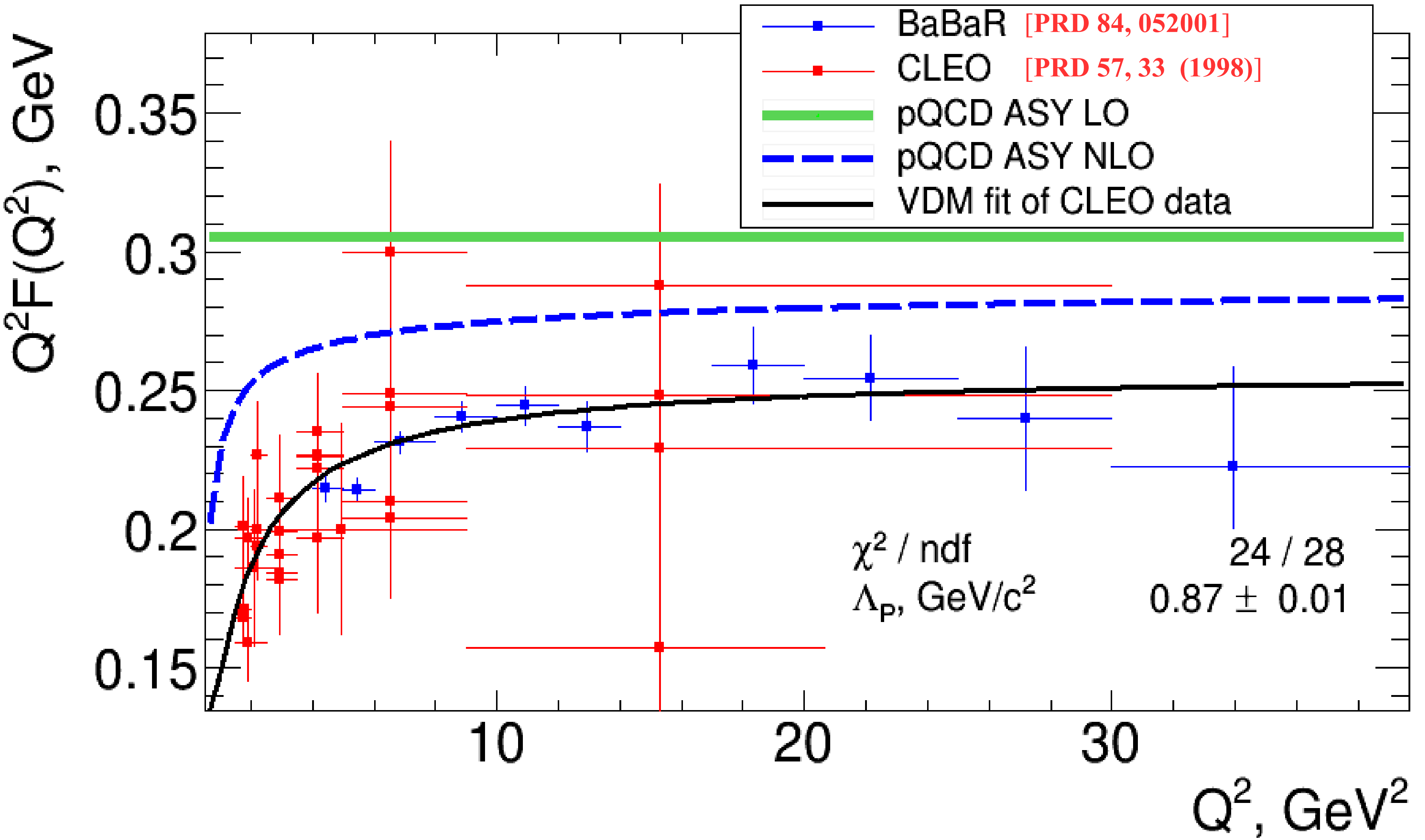

The $\gamma^*\gamma \rightarrow \eta$ Transition Form Factor

The analysis is based on the previous BaBar study [1].

previous

$\gamma\gamma^* \to \eta'$
Single tagged
~ 5000 signal events

new

$\gamma^*\gamma^* \to \eta'$
Double tagged
46^{+8}_{-7} signal events

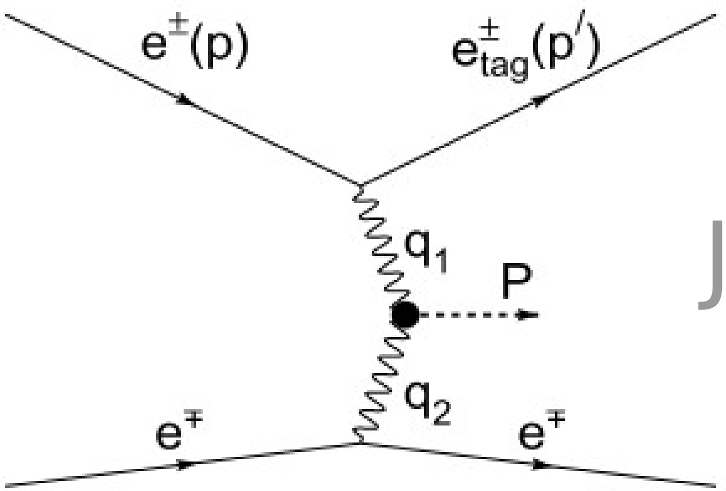

$J^{PC} = 0^{-+}$

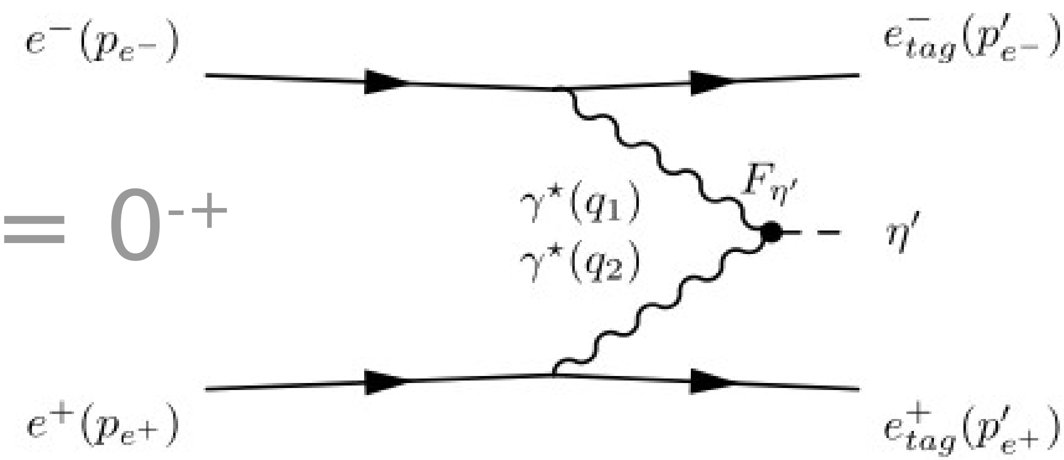

- **A large number of systematic uncertainties were studied in our previous work where the number of signal events was significantly larger.**

[1] [PRD 84, 052001]: **P. del Amo Sanchez *et al. (BaBar collaboration),* Phys. Rev. D 84, 052001 (2011) — (126 citations).**

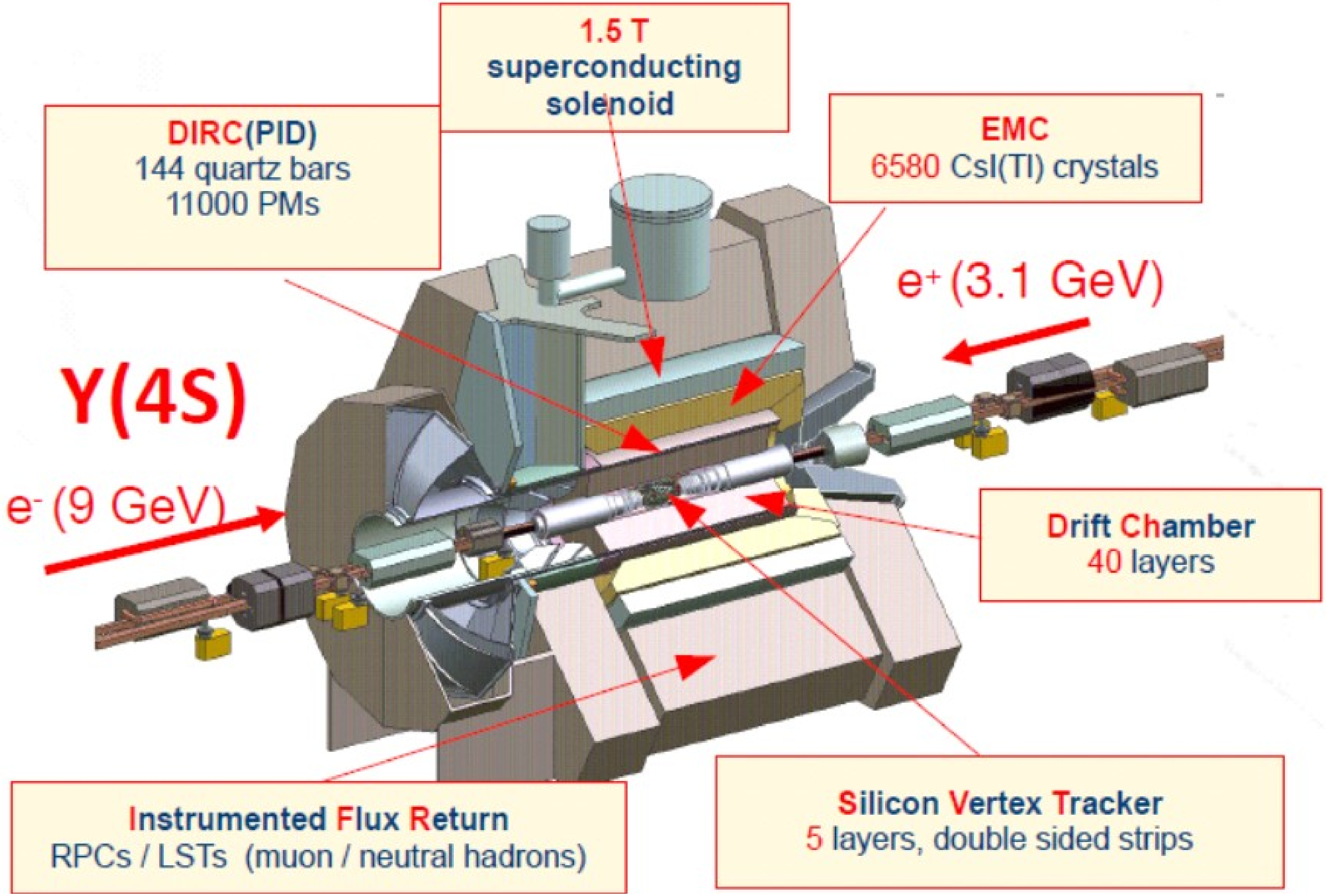

BABAR detector at center-of mass energy of 10.6 GeV at the e^+e^- collider PEP-II at SLAC

$$q^2_{e^-} = -Q^2_{e^-} = (p_{e^-} - p'_{e^-})^2$$

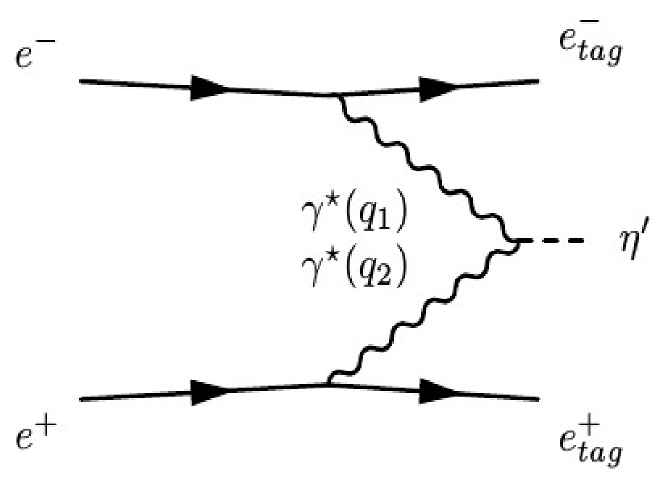

$$q^2_{e^+} = -Q^2_{e^+} = (p_{e^+} - p'_{e^+})^2$$

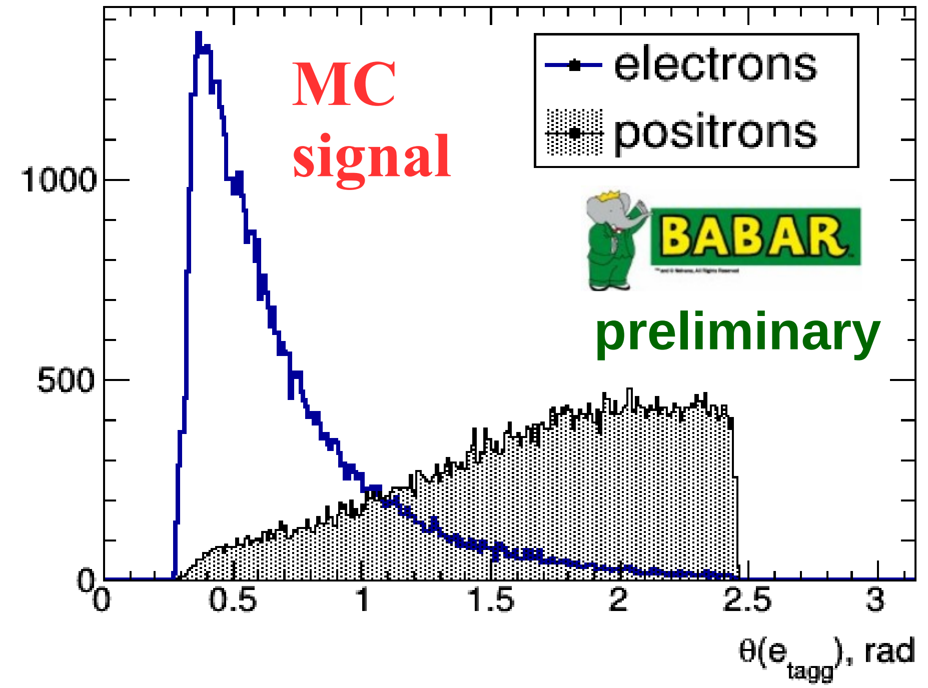

Polar angle distribution for tagged electrons (positrons)

- The decay chain $\eta' \to \pi^+\pi^-\eta \to \boldsymbol{\pi^+\pi^- 2\gamma}$ is used
- A total integrated luminosity L = 469 fb^{-1}
- GGResRc event generator is used [arXiv:1010.5969]. Initial and final state radiative corrections as well as vacuum polarization effects are included. The form factor is fixed to the constant value F(0,0).

The strategy: $dN/dQ^2 \rightarrow d\sigma/dQ^2 \rightarrow |F(Q^2)|$

- The total reconstructed **momentum** of $e^+e^-\pi^+\pi^-\eta$ system in c.m. frame is less than 0.35 GeV/c.

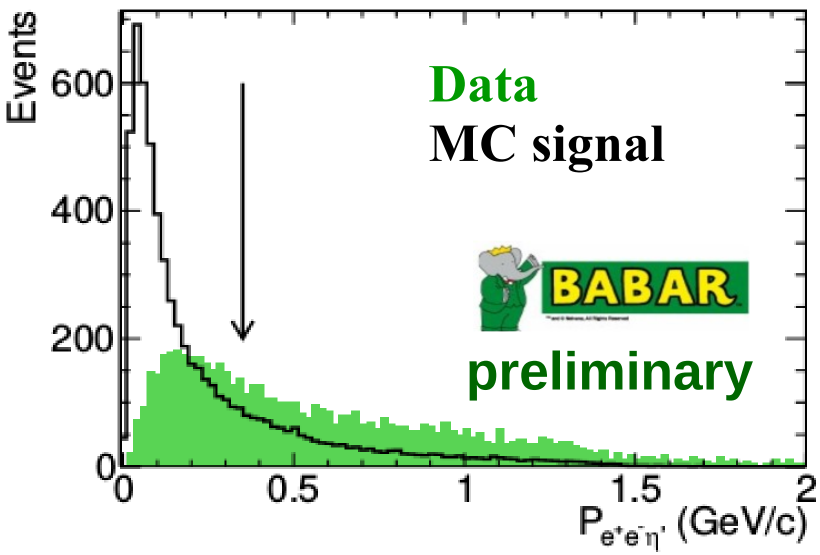

- The total reconstructed **energy** of $e^+e^-\pi^+\pi^-\eta$ system in c.m. frame belongs to the range [10.3:10.7] GeV

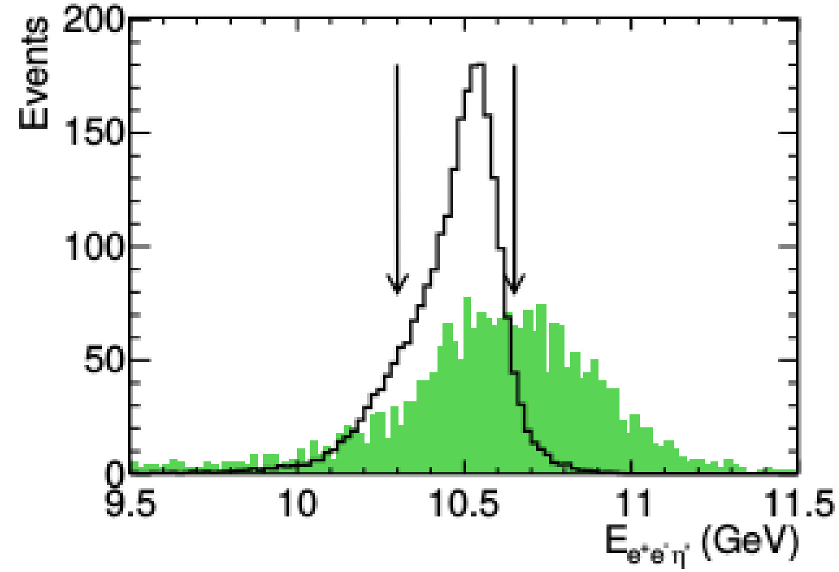

- Events that lie above and on the right of the lines (mostly, Bhabha scattering) are rejected.

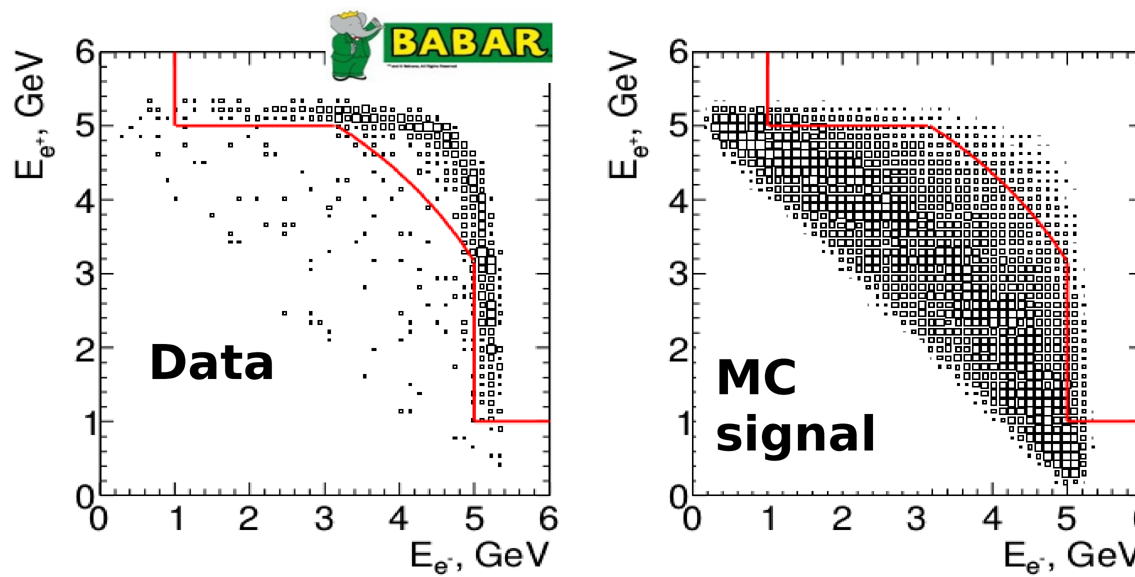

The positron c.m. energy vs. the electron c.m. energy

Event selection

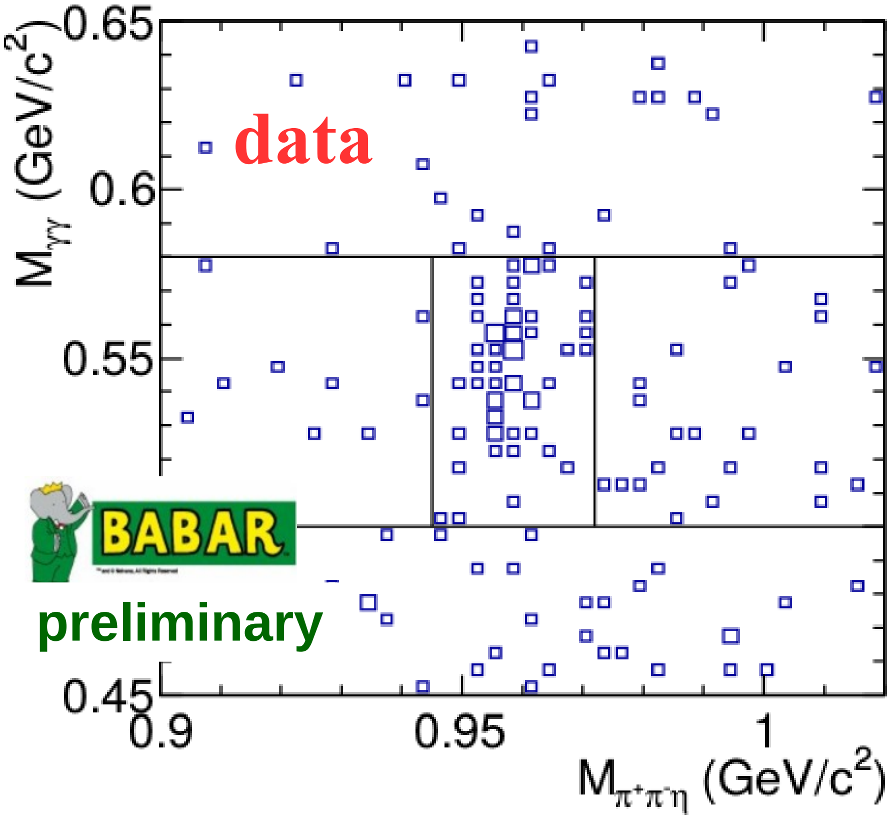

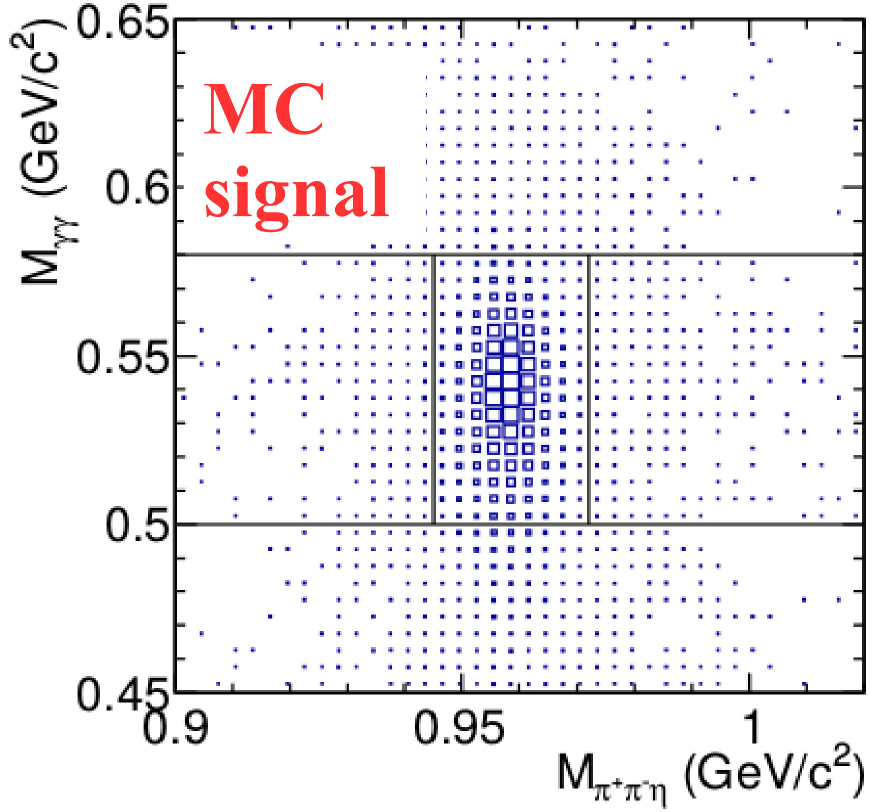

$$m_{\gamma\gamma}\ vs.\ m_{\pi+\pi-\eta}$$

- We require $0.50 < m_{\gamma\gamma} < 0.58$ GeV/c^2

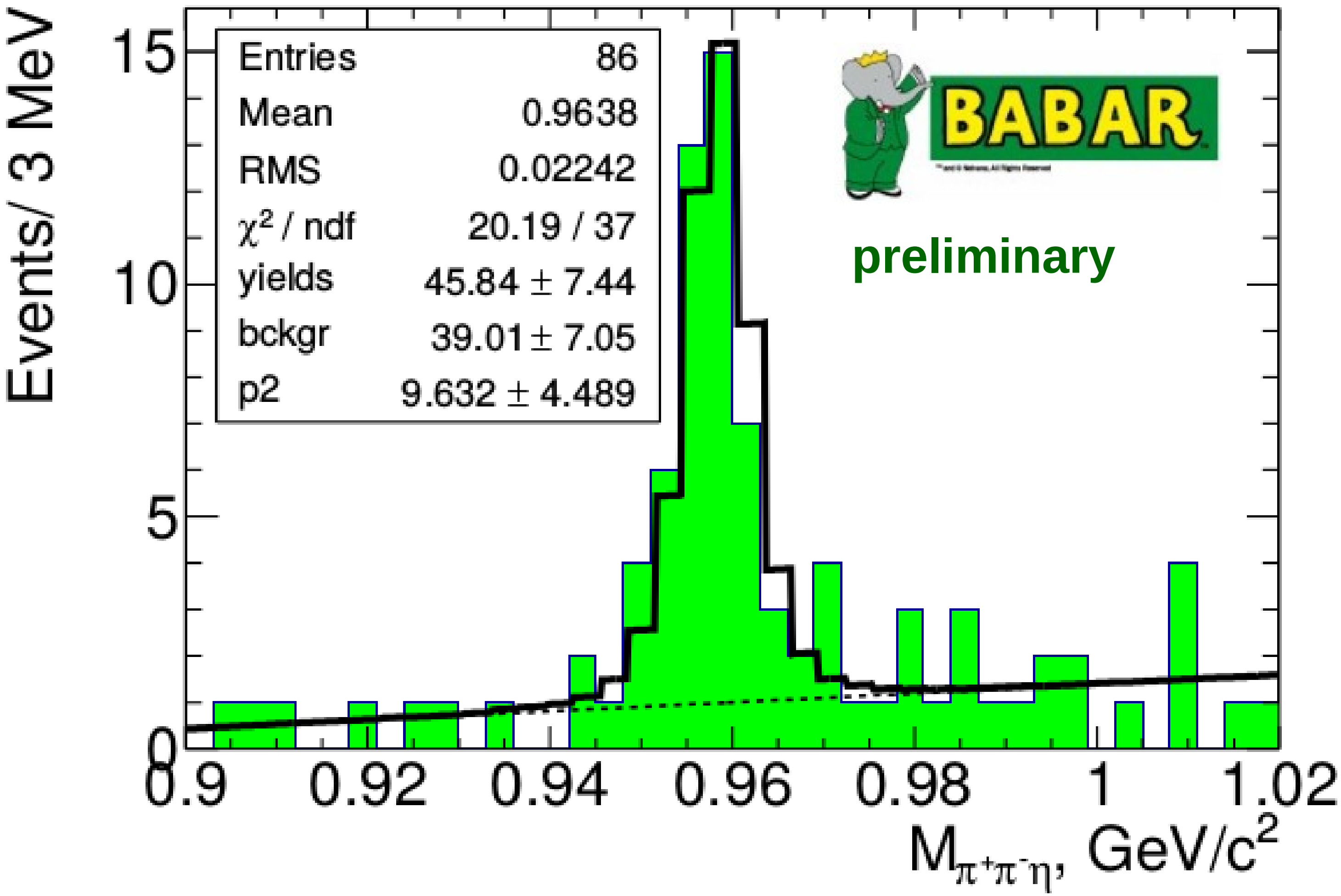

The $\pi^+\pi^-\eta$ mass spectra for data events. The open histogram is the fit result. The dashed line represents fitted background.

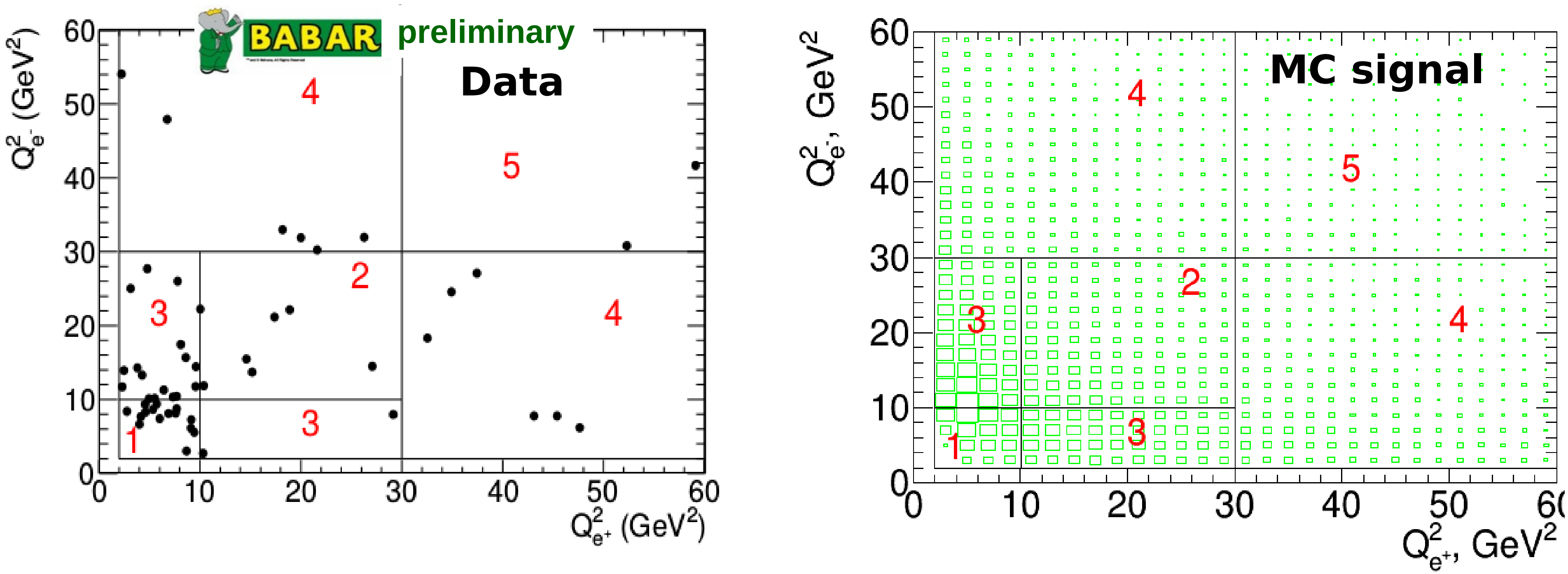

The Q^2_{e-} *vs.* Q^2_{e+} *for events with* $\mathbf{0.945 < m_{2\pi\eta} < 0.972}$ GeV/c^2

- New definition: $Q_1^2 = \max(Q_{e+}^2, Q_{e-}^2),\ Q_2^2 = \min(Q_{e+}^2, Q_{e-}^2)$

- The average momentum transfers for each region are calculated using the data spectrum normalized to the detection efficiency:

$$\overline{Q_{1,2}^2} = \frac{\sum_i Q_{1,2}^2(i)/\varepsilon(Q_1^2, Q_2^2)}{\sum_i 1/\varepsilon(Q_1^2, Q_2^2)}.$$

- The total number of signal events $\mathbf{N^{fit}_{signal} = 46.2^{+8.3}_{-7.0}}$

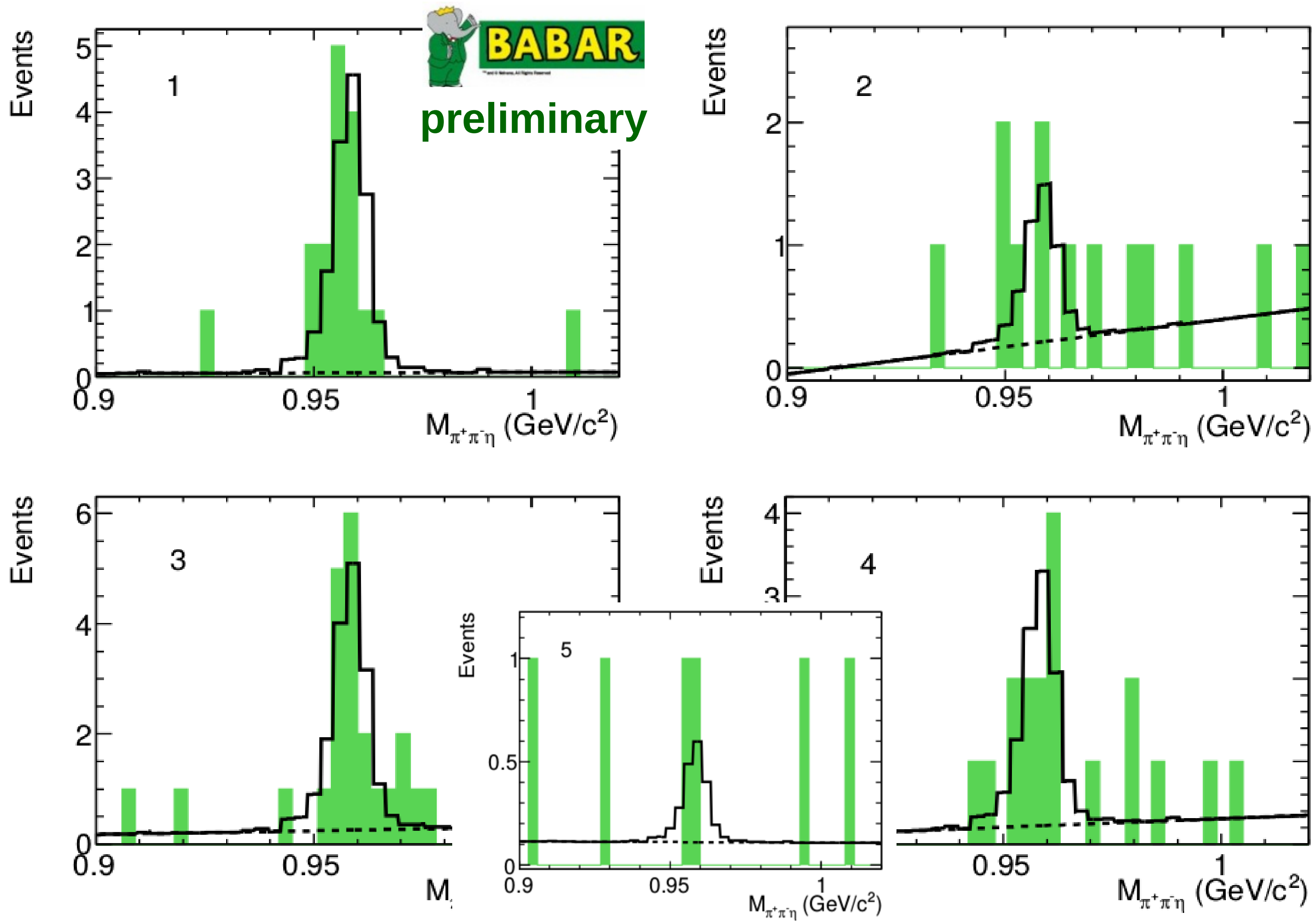

The $\pi^+\pi^-\eta$ mass spectra for data events for the five Q^2 ranges. The open histograms are the fit results. The dashed lines represent background.

Detection efficiency

- The detector acceptance limits the e^-e^+ detection efficiency at small Q^2 . The minimum Q^2 equals to 2 GeV^2.

$$\varepsilon_{true} = \frac{\int \varepsilon(Q_1^2, Q_2^2) F^2_{\eta'}(Q_1^2, Q_2^2) dQ_1^2 dQ_2^2}{\int F^2_{\eta'}(Q_1^2, Q_2^2) dQ_1^2 dQ_2^2}$$

($\boldsymbol{F_{\eta'}}$ from *master formula* at slide #7)

BABAR preliminary

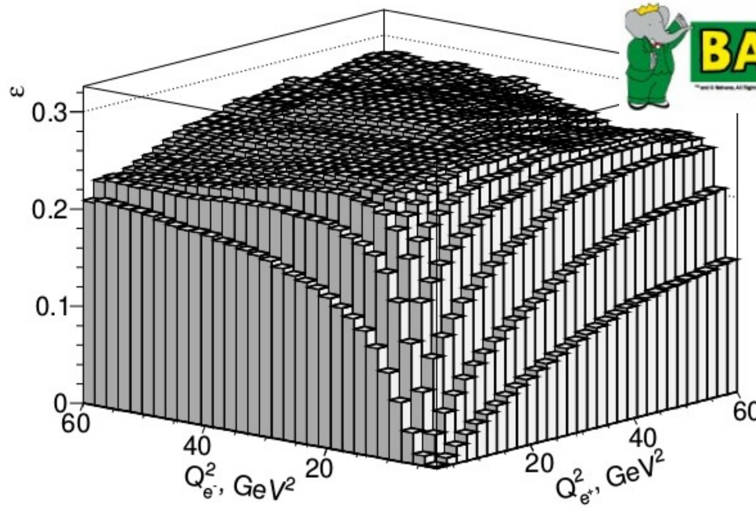

The dependence of detection efficiency on momentum transfers.

- Radiative corrections $R(Q_1^2, Q_2^2) = \dfrac{\sigma^{rad}(Q_1^2, Q_2^2)}{\sigma^{born}(Q_1^2, Q_2^2)}$

- R leads to the decrease of the detection efficiency by ~ 15 %.

- The maximum energy of the photon emitted from the initial state is restricted by the requirement $E_\gamma < 0.05\sqrt{s}$, where $\sqrt{s}$ is the e^+e^- center-of-mass (c.m.) energy.

- The differential cross section for $e^+e^- \to e^+e^-\eta'$ is calculated as

$$\frac{d^2\sigma}{dQ_1^2 dQ_2^2} = \frac{1}{\varepsilon_{\text{true}} RLB} \frac{d^2 N}{dQ_1^2 dQ_2^2}$$

$$F^2(\overline{Q_1^2}, \overline{Q_2^2}) = \frac{(d^2\sigma/(dQ_1^2 dQ_2^2))_{data}}{(d^2\sigma/(dQ_1^2 dQ_2^2))_{MC}} F^2_{\eta'}(\overline{Q_1^2}, \overline{Q_2^2})$$

- $B = B(\eta' \to \pi^+\pi^-\eta) \times B(\eta \to 2\gamma) = (0.3941 \pm 0.0020) \times (0.429 \pm 0.007) = 0.169 \pm 0.003$

- $\boldsymbol{\sigma_{e+e-\to e+e-\eta'}}$ **$(2 < Q_1^2, Q_2^2 < 60$ GeV$^2) = (11.4^{+2.8}_{-2.4})$ fb**

$\overline{Q_1^2}, \overline{Q_2^2}$, GeV^2	$\varepsilon_{\text{true}}$	R	N_{events}	$d^2\sigma/(dQ_1^2 dQ_2^2)$ $\times 10^4$, fb/GeV^4	$F(\overline{Q_1^2}, \overline{Q_2^2})$ $\times 10^3$, GeV^{-1}
6.48, 6.48	0.019	1.03	$14.7^{+4.3}_{-3.6}$	$1471.8^{+430.1}_{-362.9}$	$14.32^{+1.95}_{-1.89} \pm 0.83 \pm 0.14$
16.85, 16.85	0.282	1.10	$4.1^{+2.7}_{-2.7}$	$4.2^{+2.8}_{-2.8}$	$5.35^{+1.54}_{-1.54} \pm 0.31 \pm 0.42$
14.83, 4.27	0.145	1.07	$15.8^{+4.8}_{-4.0}$	$39.7^{+12.0}_{-10.2}$	$8.24^{+1.16}_{-1.13} \pm 0.48 \pm 0.65$
38.11, 14.95	0.226	1.11	$10.0^{+3.9}_{-3.2}$	$3.0^{+1.2}_{-1.0}$	$6.07^{+1.09}_{-1.07} \pm 0.35 \pm 1.21$
45.63, 45.63	0.293	1.22	$1.6^{+1.8}_{-1.1}$	$0.6^{+0.7}_{-0.6}$	$8.71^{+3.96}_{-8.71} \pm 0.50 \pm 1.04$

Statistical **Systematic** **Model**

- Statistical uncertainty is dominated

- **$e^+e^-\to e^+e^-\eta'\pi^0\to e^+e^-\pi^-\pi^+\eta\pi^0$** - kinematically closest background for the process under study. Using the simulation of the $e^+e^-\to e^+e^-a_0(1450)\to e^+e^-\eta'\pi^0$ process we estimate the contribution $N_{\eta'\pi 0} < 0.16$ at 90% C.L.

- **$e^+e^-\to e^+e^-J/\psi(\varphi)\to e^+e^-\eta'\gamma$** as well as **$e^+e^-\to\gamma^*\to X$** are also negligible.

- The systematic uncertainty (12%) of cross section is dominated by the uncertainty related to selection criteria (11%).

- Predominantly, the model uncertainty arises from the model dependence of $\mathbf{(d^2\sigma/(dQ^2_1\ dQ^2_2))_{MC}}$ and $\boldsymbol{\varepsilon_{true}}$.

  Repeating the calculations with a constant TFF we estimate the model uncertainty.

  For the cross section - about 60% due to the strong dependence of ε_{true} on the input model for TFF at small values of Q^2_1 and Q^2_2.

  However, the TFF is much less sensitive to the model.

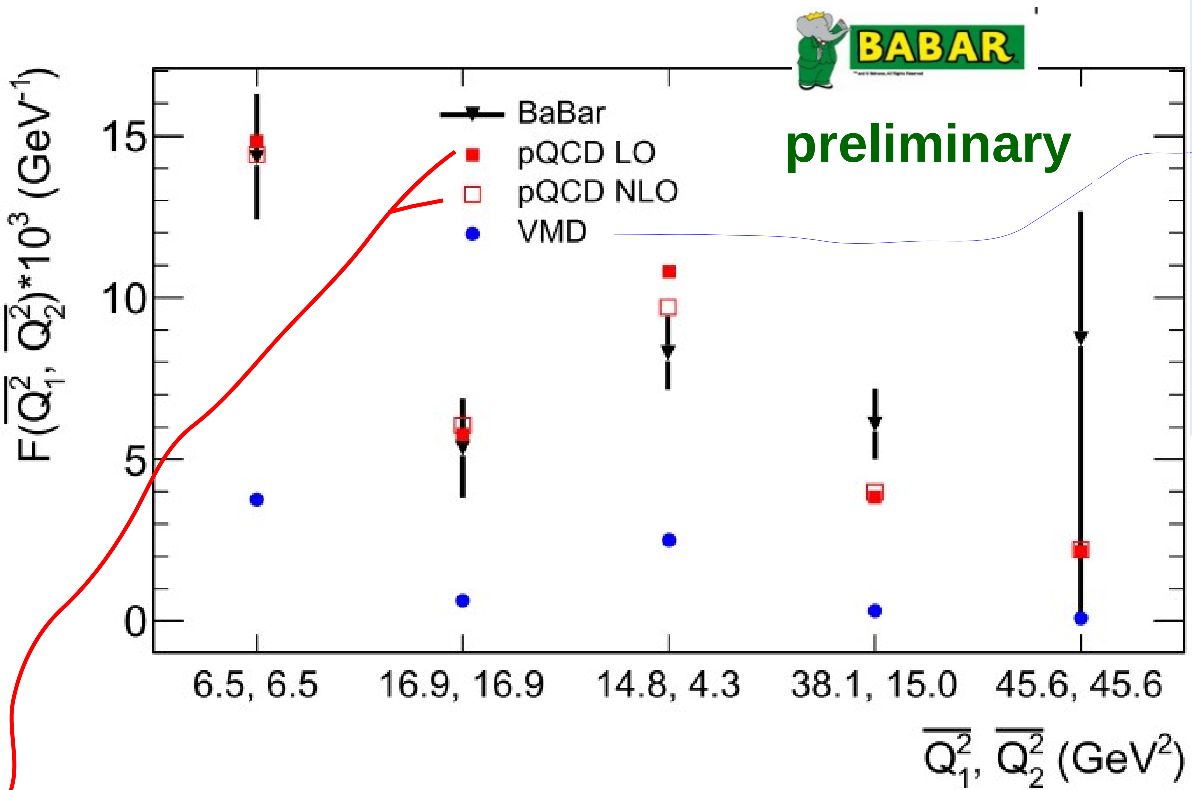

$$F_{\eta'}(Q_1^2, Q_2^2) = \frac{F_{\eta'}(0,0)}{(1 + Q_1^2/\Lambda_P^2)(1 + Q_2^2/\Lambda_P^2)}$$

The Λ_P is fixed at 849 MeV/c² from the approximation of $F_{\eta'}(Q^2, 0)$ with one off-shell photon [Phys. Rev. D 85, 057501 (2012)].

The comparison of obtained form-factor with theoretical predictions

LO

$$F_{\eta'}(Q_1^2, Q_2^2) = \left(\frac{5\sqrt{2}}{9} f_n \sin\phi + \frac{2}{9} f_s \cos\phi\right) \int_0^1 dx \frac{1}{2} \frac{6x(1-x)}{xQ_1^2 + (1-x)Q_2^2} \left(1 + C_F \frac{\alpha_s(\mu^2)}{2\pi} \cdot t(x, Q_1^2, Q_2^2)\right) + (x \to 1-x),$$

NLO

- pQCD calculation is in good agreement with data (χ^2/n.d.f. = 6.2/5, Prob = 28%)
- VMD model exhibits a clear disagreement with the experiment

preliminary

- **About 46 events of $e^+e^- \rightarrow e^+e^-\eta'$ were preliminary observed in the double tagged mode for the first time.**

- **The $\gamma^*\gamma^*\rightarrow\eta'$ transition form factor $F(Q^2_1, Q^2_2)$ have been preliminary measured for Q^2 range from 2 to 60 GeV^2.**

- **The form factor is in reasonable agreement with the pQCD prediction and contradicts the prediction of the VMD model.**

Thank you!

Back up slides

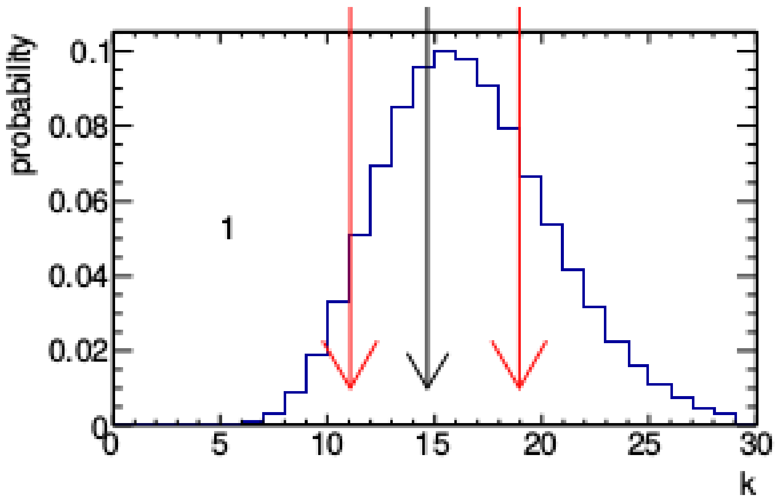

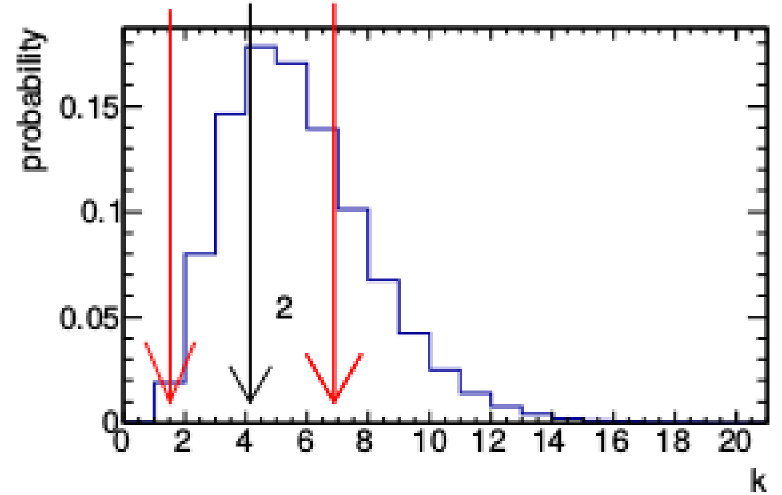

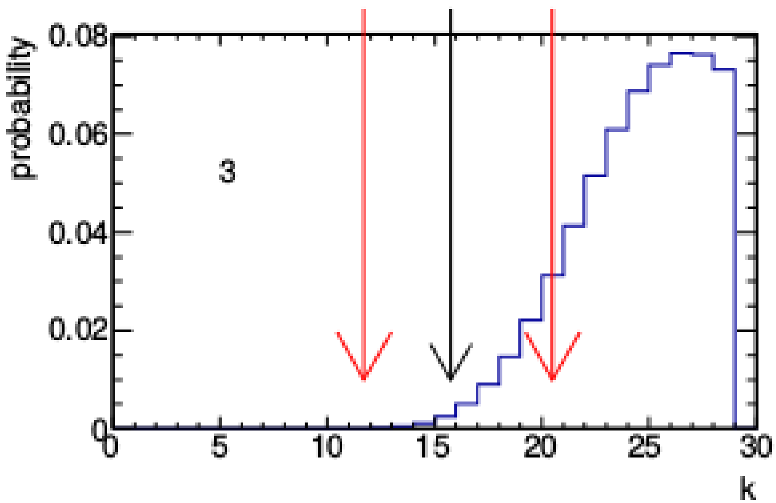

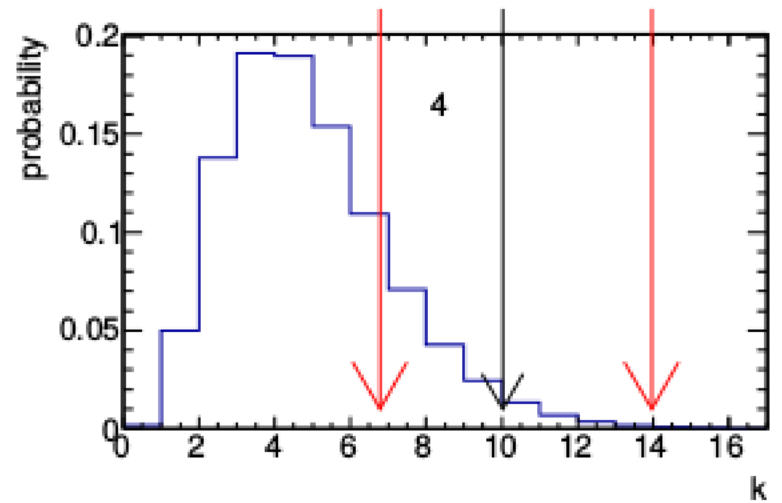

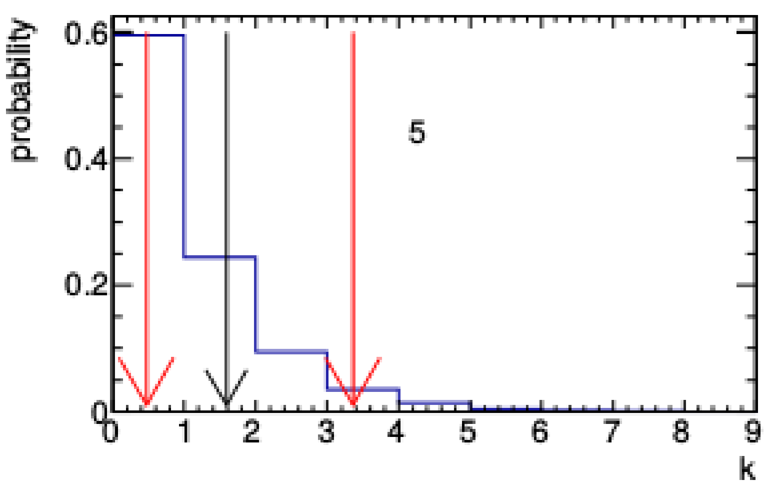

k — Poisson probability for k number of events to be detected according to pQCD;

Black arrow — the number of observed signal events;

Red arrows — the window of errors from fit.

- $e^+e^-\to e^+e^-\eta'\pi^0\to e^+e^-\pi^-\pi^+\eta\pi^0$ - kinematically closest background for the process under study.

- We perform the search of the process using all BaBar data and the same technique as for $e^+e^-\to e^+e^-\eta'$ with additional requirements for π^0.

- We simulate the process via the mechanism $e^+e^-\to e^+e^-a_0(1450)\to e^+e^-\eta'\pi^0$. More details can be found in BAD#2689.

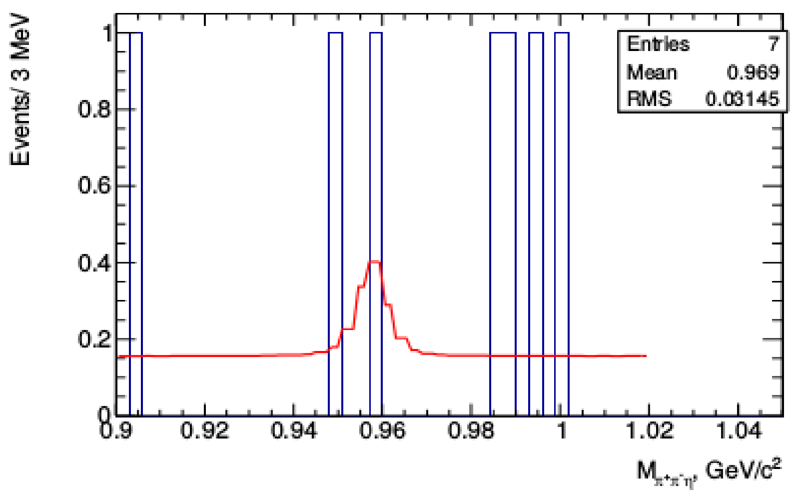

The $\pi^+\pi^-\eta$ invariant mass spectrum

$$N^{signal}_{\eta'\pi^0} < 1.45 \text{ at } 90\% \text{ C.L.}$$

The detection efficiency for $e^+e^-\eta'\pi^0$ events to pass the selections of **$e^+e^-\eta'$.**

$$N_{bkgr} = \frac{N^{signal}_{\eta'\pi^0}\,\epsilon^{(2)}_{\eta'\pi^0}}{\epsilon^{(1)}_{\eta'\pi^0}} < 0.16 \text{ at } 90\% \text{ C.L.}$$

The detection efficiency for $e^+e^-\eta'\pi^0$ events to pass the selections of **$e^+e^-\eta'\pi^0$.**

Systematic uncertainty

The main source of systematic uncertainty of cross section

Source	Uncertainty (%)
$\pi^{\pm}$ identification	1.0
$e^{\pm}$ identification	1.0
Other selection criteria	11
Track reconstruction	0.9
$\eta \to 2\gamma$ reconstruction	2
Trigger, filters	1.3
Background subtraction	3.7
Radiative correction	1.0
Luminosity	1.0
Total	12%

from previous BaBar study of $\gamma^*\gamma\to\eta'$
Phys. Rev. D 74 012002 (2006)

TABLE IV: The result of the study of the uncertainty associated with the selection criteria

selection	$N_{signal}/\varepsilon_{true}$	deviation from standard criteria
standard selection criteria	985 ± 197	
$P_{e^+e^-\eta'}$ is less than 1 GeV/c instead of 0.35 GeV/c	1052 ± 273	6.8
$10.20 < E_{e^+e^-\eta'} < 10.75$ GeV instead of $10.3 < E_{e^+e^-\eta'} < 10.65$ GeV	942 ± 235	-4.3
without the restrictions on E_{e^+} and E_{e^-}	1061 ± 280	7.7
$0.48 < m_{2\gamma} < 0.60$ GeV/c^2 instead of $0.50 < m_{2\gamma} < 0.58$ GeV/c^2	958 ± 181	-2.7
total		11

- $e^+e^- \to e^+e^- J/\psi(\varphi) \to e^+e^- \eta'\gamma$ is negligible according to [**PRD 84, 052001].**

- $e^+e^- \to \gamma^* \to X$

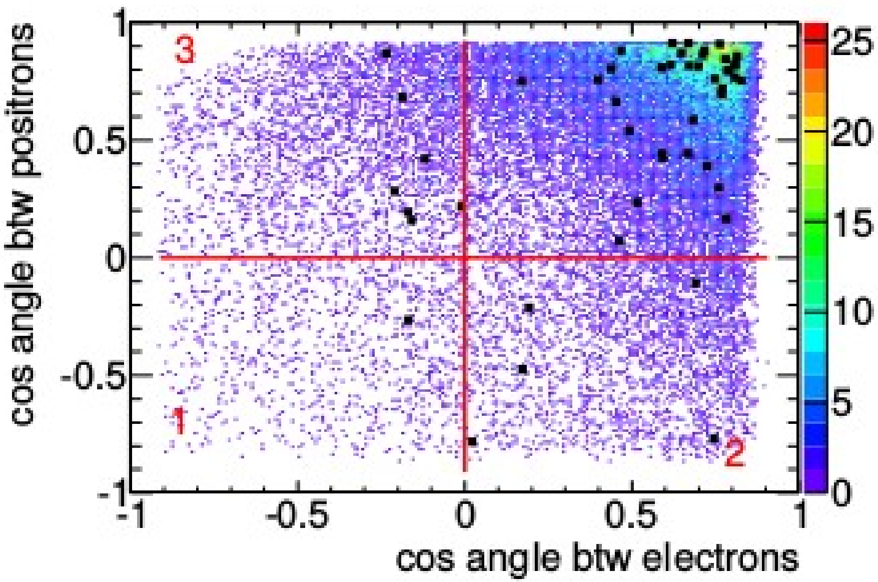

The cosine of angle between scattered and initial electron (positron) in c.m.f.

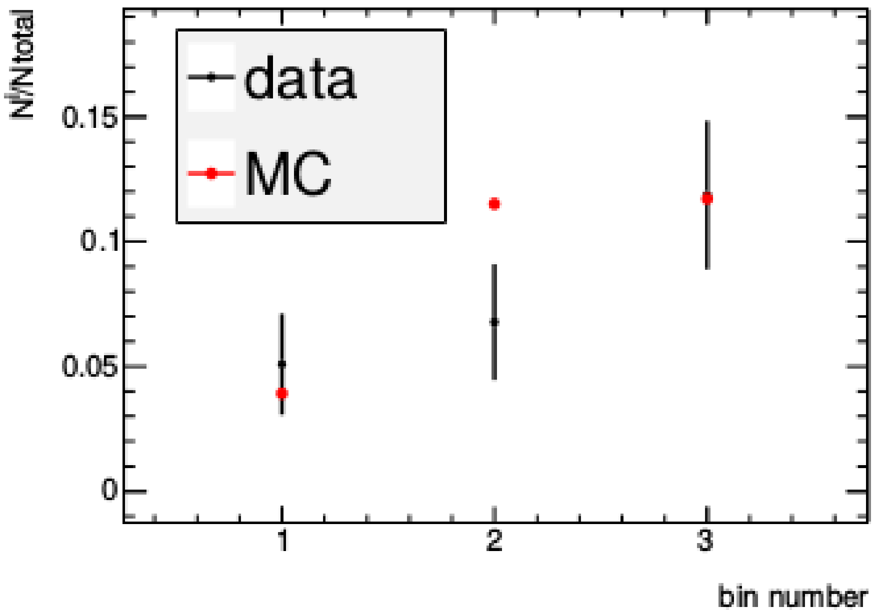

The fraction of the events in the bins.

It is reasonable to assume that the $\cos(\alpha_{e\pm})$ spectrums must be symmetric in [-1:1] region for **annihilation processes**, while signal scattered electron (positron) prefers to fly in the about the same direction.

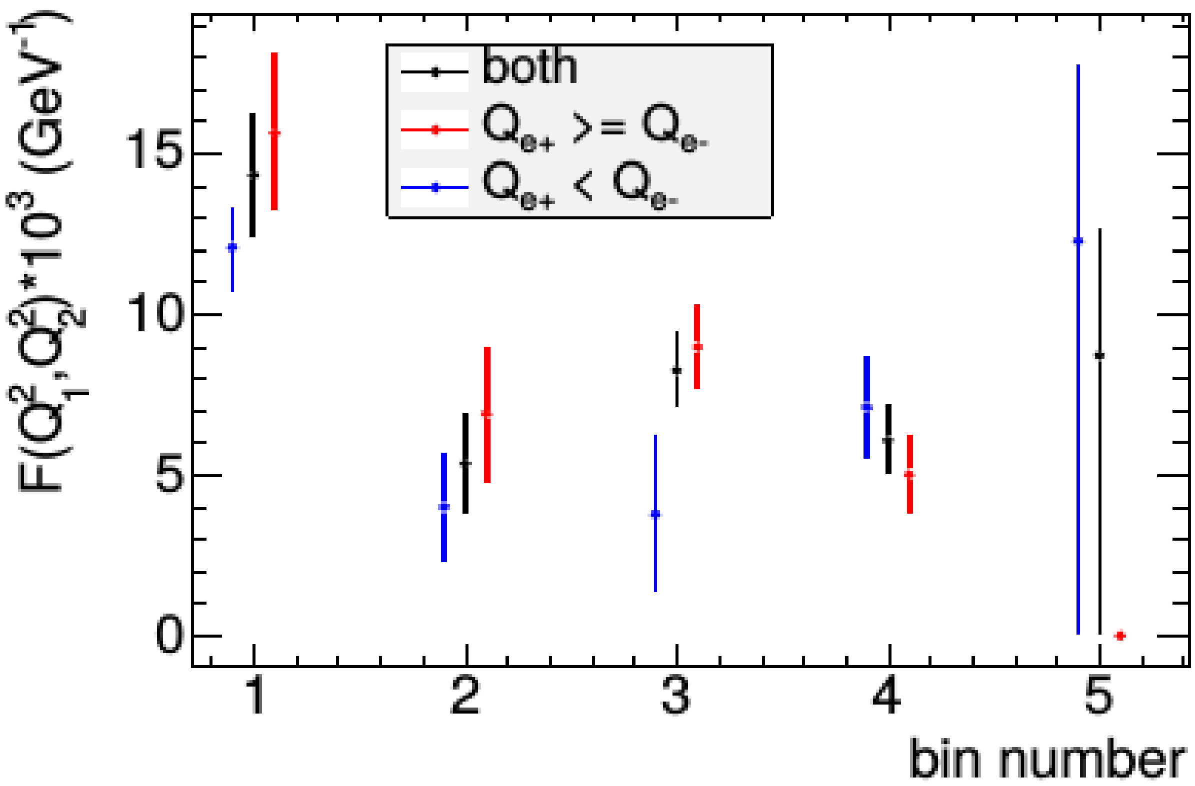

The comparison of the measured η′ TFF with $Q^2_{e+} < Q^2_{e-}$, $Q^2_{e+} >= Q^2_{e-}$ and without the restriction.

Event selection

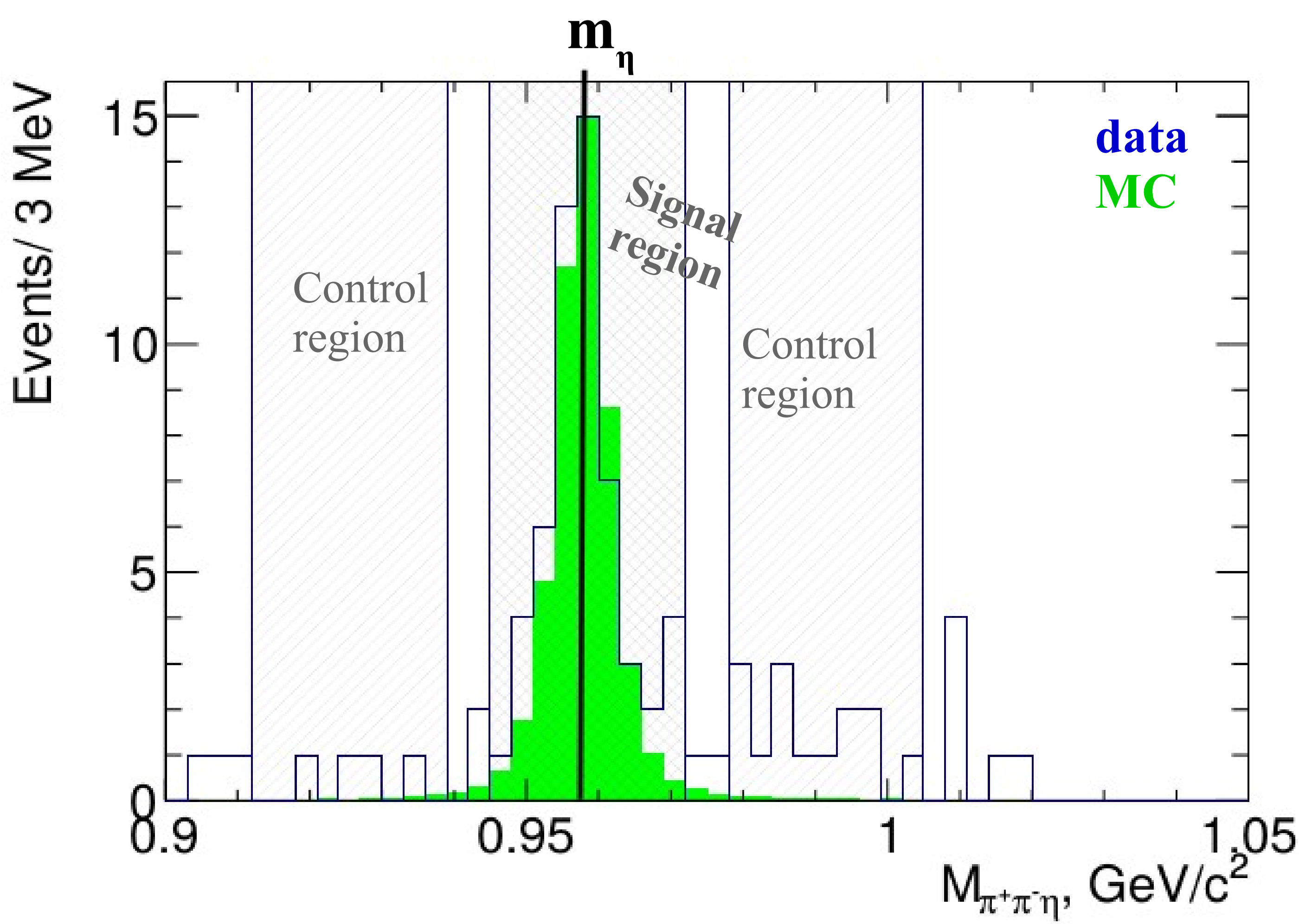

The data-MC comparison of ππη invariant mass distribution. The MC histogram is normalized to central bin of data distribution.

The expected number of signal $\mathbf{N}^{\mathbf{side}}_{\mathbf{signal}}$ = 55 - 18/2 = 46

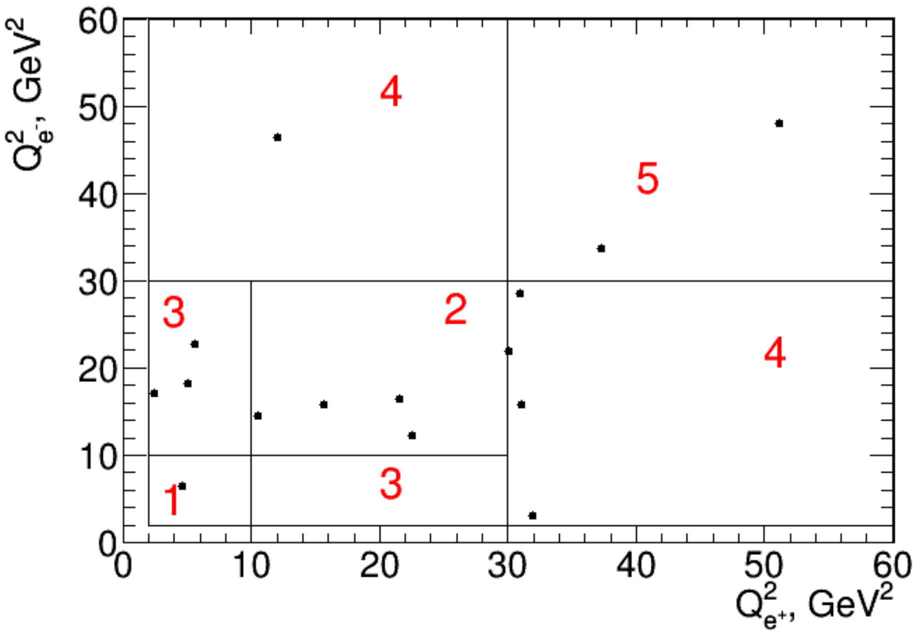

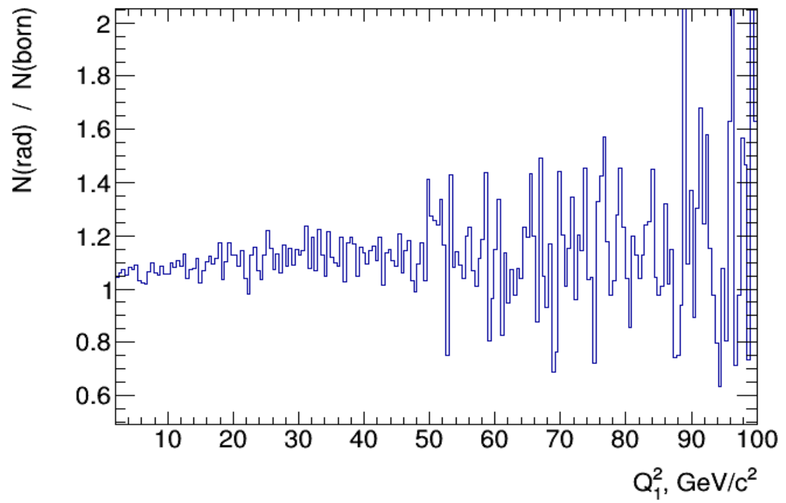

The ratio of generated spectra with rad. photons vs. without photons

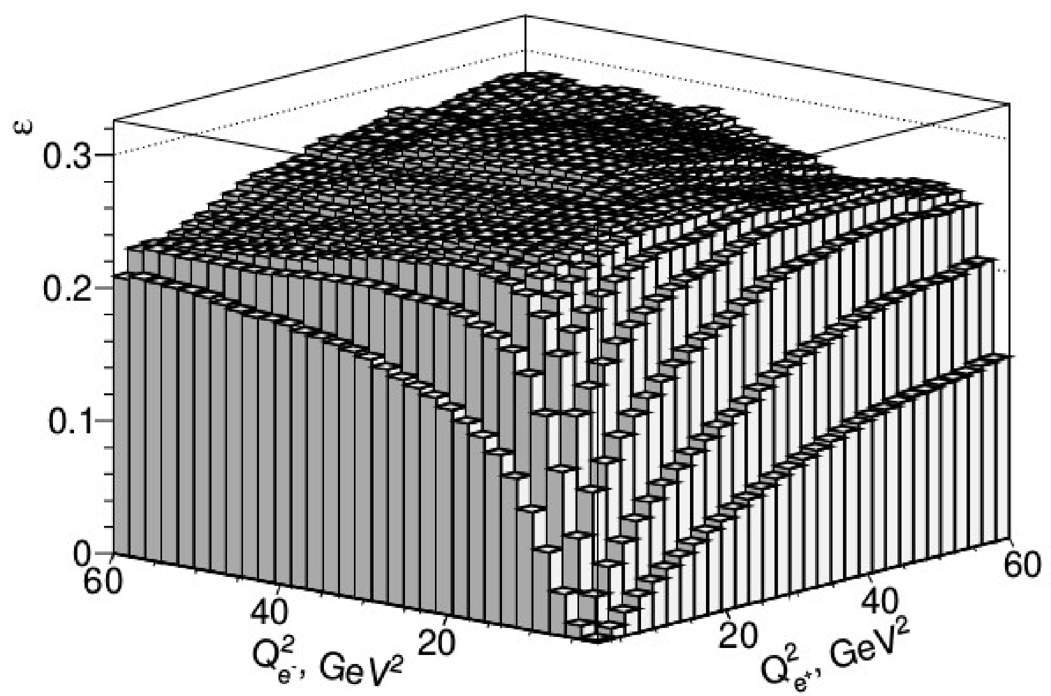

The dependence of detection efficiency on momentum transfers.

We require the presense

- at least **two tracks** from *GoodTrackLoose* list passed *LooseElectronMicroSecection*
  - $0.3 < \theta_e < 2.45$ radians

- at least **two tracks** from *GoodTrackLoose* list passed TightKMPionMicroSelection
  - $0.45 < \theta_\pi < 2.4$ radians

- at least **two photons** from *GoodPhotonLoose* list
  - $\varepsilon_\gamma > 30$ MeV
  - $0.45 < m_{\gamma\gamma} < 0.65$ GeV/c^2
  - The photon candidates are fitted with a η mass constraint.

- The η candidate and a pair of oppositely-charged pion candidates are fitted with a η' mass constraint.

TABLE V: $\frac{d^2\sigma}{dQ_1^2 dQ_2^2}$ obtained with different models for TFF

	1	2	3	4	5
QCD	$1471.8^{+430.136}_{-362.91}$	$4.17^{+2.75}_{2.75}$	$39.72^{+11.98}_{-10.18}$	$2.98^{+1.17}_{-0.96}$	$0.62^{+0.69}_{-0.62}$
const	$637.10^{+186.19}_{-157.09}$	$4.15^{+2.74}_{2.74}$	$33.30^{+10.05}_{-8.54}$	$2.76^{+1.08}_{-0.89}$	$0.62^{+0.69}_{-0.62}$
deviation, %	60	0.6	15	7	1.

TABLE VI: TFF obtained with different models for TFF

	1	2	3	4	5
QCD	$14.32^{+1.95}_{-1.89}$	$5.35^{+1.54}_{-1.54}$	$8.24^{+1.16}_{-1.13}$	$6.07^{+1.09}_{-1.07}$	$8.71^{+3.96}_{-8.71}$
const	$14.61^{+1.99}_{-1.92}$	$5.62^{+1.62}_{-1.62}$	$7.24^{+1.02}_{-0.99}$	$7.24^{+1.30}_{-1.28}$	$10.02^{+4.55}_{-10.02}$
deviation %	1	8	8	20	12